Computer simulation study of a mesogenic lattice model based on long-range dispersion interactions

Silvano Romano[*]

Physics Department, University of Pavia, via A. Bassi 6, 27100 Pavia, Italy
(Received 24 July 2016; published 18 October 2016)

In contrast to thermotropic biaxial nematic phases, for which some long sought for experimental realizations have been obtained, no experimental realizations are yet known for their tetrahedratic and cubatic counterparts, involving orientational orders of ranks 3 and 4, respectively, also studied theoretically over the last few decades. In previous studies, cubatic order has been found for hard-core or continuous models consisting of particles possessing cubic or nearly cubic tetragonal or orthorhombic symmetries; in a few cases, hard-core models involving uniaxial ($D_{\infty h}$-symmetric) particles have been claimed to produce cubatic order as well. Here we address by Monte Carlo simulation a lattice model consisting of uniaxial particles coupled by long-range dispersion interactions of the London-De Boer-Heller type; the model was found to produce no second-rank nematic but only fourth-rank cubatic order, in contrast to the nematic behavior long known for its counterpart with interactions truncated at nearest-neighbor separation.

I. INTRODUCTION

Thermotropic biaxial nematic liquid crystals have been called "the holy grail" of liquid crystal research, both for fundamental reasons and in connection with their possible technological applications in displays [1]; a coherent pedagogical account of background and present state of the art on the subject has been published in 2015 [2], and we refer to it for a more detailed discussion and more extensive bibliography of the different aspects of this fascinating and challenging subject.

Here we briefly recall that nematic phases are usually apolar and uniaxial ($D_{\infty h}$-symmetric), although the constituent molecules possess lower symmetries; biaxiality was discovered in a smectic C phase in 1970 [3], and, in the same year, Freiser [4] addressed the possibility of biaxial mesogenic molecules producing a biaxial nematic phase; the following years saw extensive theoretical and simulation investigations to elucidate the properties of the hypothetical biaxial phase (especially in theoretical work, molecular D_{2h} symmetry has mostly been studied, but lower symmetries have been addressed as well in recent years [5]). There also followed several attempts to produce experimental realizations, which remained unsuccessful until the end of the past century; better evidence was obtained over the last 12 years [5,6]; in these cases, second-rank orientational order is involved.

On the other hand, the theoretical possibility of positional disorder accompanied by orientational order of other point-group symmetries, involving tensors of rank L different from 2, has been investigated theoretically for some 30 years to date [7–10], especially for tetrahedratic ($L = 3$) and cubatic orders ($L = 4$); a detailed symmetry classification of "unconventional" nematic phases, i.e., associated with the onset of either one tensor of rank different from 2 or of several combined tensors, has been carried out by Mettout [10]; a general classification of point-group symmetric orientational ordering tensors has recently been published [11]. This line of investigations has partly overlapped with the study of packings of hard nonspherical particles, including a number of polyhedra (see, e.g., Refs. [12–18]): in addition to the extensive search for the densest packing obtainable for a specific particle geometry, resulting phase diagrams (including possible mesophases) have been studied.

The possibility of tetrahedratic orientational order, involving a third–rank order parameter, was proposed and studied by L. G. Fel [8,9]; its transitional behavior was later studied by Lubensky and Radzihovsky [19,20], and the macroscopic consequences of tetrahedratic order were discussed in detail by Brand *et al.* [21–23]. Continuous interaction lattice models involving third-rank interactions alone [24] or combined with second-rank terms [25,26] and producing tetrahedratic order have also been studied by simulation. Starting in the mid-1990s, bent-core (banana-shaped) mesogens were synthesized [27] and found to produce mostly smectic and sometimes nematic [28] phases; to the best of our knowledge, no experimental realizations of a purely tetrahedratic phase are known at present, and no third–rank order parameter has been measured to date, yet the theoretical analyses in Refs. [19–23] show that interactions of tetrahedral symmetry (or, in more general terms, a description allowing for first-, second-, and third-rank ordering tensors) are needed for the proper comprehension of macroscopic properties of mesophases resulting from bent-core molecules. Some experimental evidence suggesting tetrahedratic behavior in an achiral bent-core liquid crystal has been reported in Ref. [29].

Over the last decades, the possible existence of a cubatic mesophase, possessing cubic orientational order (i.e., along three equivalent mutually orthogonal axes) but no translational one, has been extensively investigated by approximate analytical theories and by simulation [30–43] and explicitly predicted in some cases; hard-core models possessing cubic or nearly cubic tetragonal or orthorhombic symmetries have been studied rather extensively: for example, Onsager crosses were studied in Ref. [34], and tetrapods were investigated in Ref. [35]; arrays of hard spheres with tetragonal or cubic symmetries have been studied in Refs. [36–38]; and continuous interaction models possessing cubic symmetry have been studied as well [39]. Hard-core models involving

―――――
[*]Silvano.Romano@pv.infn.it

uniaxial particles have also been investigated [30–33], [40–42]: no cubatic order was found for hard cylinders [33], whereas symmetrically cut hard spheres [30,40–42] of appropriate length-to-width appear to produce a metastable cubatic phase.

As hinted above, no experimental realizations of a thermotropic cubatic phase are known at present; on the other hand, liquid crystal phase transitions in suspension of mineral colloids [44] have been investigated for some 90 years, and evidence of cubatic order has been proposed in Ref. [45], where uniform sterically stabilized hexagonal platelets of nickel (II) hydroxide had been dispersed in D_2O. A few years later, molecular dynamics simulations [43] addressed colloidal platelets with a square cross section, and consisting of fused spherical interaction centers; a stable cubatic phase was reported.

It also seems appropriate to recall that, starting with the seminal Lebwohl-Lasher simulation papers in the early 1970s [46,47], mesophases possessing no positional order, such as the nematic one(s), have often been studied by means of lattice models involving continuous interaction potentials [48,49]; this approach also yields a convenient contact with molecular field (MF) treatments of the Maier-Saupe (MS) type [50–52]. It has been pointed out [49] that usage of a lattice model reduces the number of parameters to be controlled, thus producing important savings in computer time, and, moreover, it excludes a number a competing phases (e.g., smectic ones) from the start; similar simplifications as for the possible phases are used in other theoretical treatments as well.

The present communication reports a Monte Carlo (MC) simulation study, addressing and revisiting a lattice model involving uniaxial particles, coupled via a long-range dispersion potential, and producing cubatic but no nematic order.

The rest of this paper is organized as follows: the interaction potential and its ground state are recalled in Sec. II; simulation aspects are briefly discussed in Sec. III; simulation results are presented in Sec. IV; and the paper is concluded in Sec. V, where results are summarized.

II. INTERACTION MODEL AND GROUND STATE

As for symbols and definitions, we are considering here three-component unit vector (classical spins), associated with the nodes of a three-dimensional simple-cubic lattice $\mathbb{Z}^3$; let $\mathbf{x}_j$ denote the coordinate vectors of lattice sites, let $\mathbf{w}_j$ denote the unit vectors, and let $w_{j,\iota}$ denote their Cartesian components with respect to an orthonormal basis $\mathcal{E} = \{\mathbf{e}_\iota, \iota = 1,2,3\}$ defined by lattice axes; the unit vectors $\mathbf{w}_j$ can also be parameterized by usual polar angles (θ_j, ϕ_j).

The quantum theory of intermolecular forces [53,54] predicts for the dipolar contribution to the dispersion energy between two identical, neutral, and centrosymmetric linear molecules the general form

$$\Delta^0_{jk} = \frac{1}{r^6}\big[g_0 + g_1\big(a_j^2 + a_k^2\big) + g_2 a_j a_k b_{jk} + g_3 b_{jk}^2 + g_4(a_j a_k)^2\big],\tag{1}$$

where

$$\mathbf{r} = \mathbf{r}_{jk} = \mathbf{x}_j - \mathbf{x}_k, \quad r = |\mathbf{r}|, \hat{\mathbf{r}} = \mathbf{r}/r,\tag{2}$$

$$a_j = \mathbf{w}_j \cdot \hat{\mathbf{r}}, \quad a_k = \mathbf{w}_k \cdot \hat{\mathbf{r}}, \quad b_{jk} = \mathbf{w}_j \cdot \mathbf{w}_k,\tag{3}$$

and the g coefficients can be calculated based on the unperturbed wave functions. Under additional simplifying approximations, Eq. (1) leads to the expression proposed by London, de Boer, and Heller (LBH) in the 1930s [55–58]:

$$\Delta_{jk} = \frac{\epsilon}{r^6}\bigg[(\gamma^2 - \gamma)S_{jk} - \frac{3}{2}\gamma^2 h_{jk} + \gamma^2 - 1\bigg],$$
$$\epsilon = \frac{3}{4}\overline{E}\overline{\alpha}^2,\tag{4}$$

where

$$h_{jk} = (3a_j a_k - b_{jk})^2, \quad S_{jk} = P_2(a_j) + P_2(a_k),$$
$$\overline{\alpha} = \frac{1}{3}(\alpha_\parallel + 2\alpha_\perp), \quad \gamma = \frac{\alpha_\parallel - \alpha_\perp}{3\overline{\alpha}}.\tag{5}$$

Here $P_2(\ldots)$ denote second Legendre polynomials of the relative arguments, $\alpha_\parallel, \alpha_\perp$ are the eigenvalues of the molecular polarizability tensor, γ denotes its relative anisotropy, and $\overline{E}$ is a mean excitation energy; formulae are also known for higher-order terms in the multipolar expansion [53,54,58]; the extreme case $\gamma = -(1/2)$ corresponds to no polarizability along the molecular symmetry axis, whereas in the other extreme $\gamma = +1$ there is polarizability along the molecular axis only. In the following, let $\tilde{\Delta}_{jk}$ denote the restriction of Δ_{jk} to nearest neighbors (n-n):

$$\tilde{\Delta}_{jk} = \epsilon\bigg[(\gamma^2 - \gamma)S_{jk} + \gamma^2\bigg(-\frac{3}{2}h_{jk} + 1\bigg)\bigg],\tag{6}$$

where a purely positional and γ-independent term appearing in Eq. (4) has been dropped.

Equation (1) or (4) has been used in the literature, usually as one component of the pair potential between comparatively simple linear molecules (see, e.g., Refs. [59–61]); limitations and possible improvements of the LBH interaction model have been discussed in the literature as well (see, e.g., Refs. [54,62]).

Models based on Eq. (6) have been investigated as possible mesogens by simulation, both on a three-dimensional (3D) [63–66] and on a two-dimensional (2D) lattice [67]; on a 3D lattice, the n-n model $\tilde{\Delta}_{jk}$ was found to produce a nematic-like ordering transition [63,66]; on the other hand, inclusion of next-nearest neighbors had been found to produce a staggered ground state structure with sublattice order but no net second-rank orientational order [64,65] (the D_3-type configurations mentioned below).

Another related mesogenic potential model, proposed by Nehring and Saupe (NS) [68], has the form

$$\Gamma_{jk} = -\frac{\epsilon}{r^6}h_{jk};\tag{7}$$

it has been used for approximate calculations of elastic properties [69,70]; its restriction to n-n, defined by

$$\tilde{\Gamma}_{jk} = \epsilon\bigg(-\frac{3}{2}h_{jk} + 1\bigg),\tag{8}$$

has later been studied by simulation in three dimensions [71,72] as well as in two dimensions [73]. Comparison between the relevant equations [Eq. (4) and (7)], shows that NS corresponds to the limiting case $\gamma = +1$ in the LBH model; actually, on a saturated cubic lattice and under periodic boundary conditions, the two models Δ_{jk} and Γ_{jk} become equivalent within purely positional terms. More explicitly, consider n-n interactions, in a periodically repeated sample, where each particle interacts with six nearest neighbors only, and the possible orientations of the intermolecular vector $\hat{\mathbf{r}}$ are $\pm \mathbf{e}_\iota, \iota = 1,2,3$; let us also recall that, for any unit vector $\mathbf{w}_j$ and for any lattice site $\mathbf{x}_j$,

$$\mathbf{w}_j \cdot \mathbf{w}_j = \sum_{\iota=1}^{3} (\mathbf{e}_\iota \cdot \mathbf{w}_j)^2, \quad \sum_{\iota=1}^{3} P_2(\mathbf{e}_\iota \cdot \mathbf{w}_j) = 0; \quad (9)$$

this identity entails that, upon summing over all interacting pairs, the terms in the pair potential containing S_{jk} cancel out identically [66,71].

Moreover, let $m = h^2 + k^2 + l^2 > 0$, denote the sum of squares of three integers, and consider the sums

$$c(m) = \sum_{\mathbf{r} \in \mathbf{Z}^3 \setminus \{\mathbf{0}\}, \mathbf{r} \cdot \mathbf{r} = m} P_2(\mathbf{w} \cdot \hat{\mathbf{r}}), \hat{\mathbf{r}} = \frac{\mathbf{r}}{|\mathbf{r}|}; \quad (10)$$

then

$$c(m) = 0, \quad (11)$$

for all m and for any unit vector $\mathbf{w}$; this result does not only hold for a simple-cubic lattice, but also for its body-centered (BCC) and face-centered (FCC) counterparts; thus, for a periodically repeated cubic sample, and for any truncation radius, the S_{jk} terms in Eq. (4) cancel out identically when summed over all interacting pairs, so that terms linear with respect to γ drop out, and only some terms proportional to γ^2 survive; in other words, in the above setting, the dispersion model Δ_{jk} [Eq. (4)] and the Nehring-Saupe model Γ_{jk} [Eq. (7)] become equivalent, within purely distance-dependent terms; the product $\epsilon \gamma^2$ in Eq. (4) or the quantity ϵ in Eq. (7) can be used to set energy and temperature scales (i.e., $T^* = k_B T/\epsilon$, where k_B denotes the Boltzmann constant).

To summarize, the present simulations, carried out on periodically repeated cubic samples, used the functional form

$$\Gamma_{jk} = +\frac{\epsilon}{r^6}\left(-\frac{3}{2}h_{jk} + 1\right), \quad (12)$$

mostly with truncation condition $\mathbf{r} \cdot \mathbf{r} \leqslant 25$.

Notice that Eq. (11), hence the equivalence between the two potential models, do not hold for a sample being finite in some direction, e.g., a 2D lattice, nor for a grand-canonical (lattice gas) simulation, where each lattice site hosts one spin at most, and its occupation number fluctuates [66,72].

A few spin configurations possessing periodicity 2 in each lattice direction and constructed as in Ref. [65] were examined as possible ground state candidates, and the results further checked by simulations carried out at low temperatures.

Procedure and definition of D_1, D_2, D_3 configurations are recalled in Appendix A for readers' convenience; let us notice that recognizing cubatic order in D_3-type configurations led to the present study.

III. COMPUTATIONAL ASPECTS

Simulations were carried out on a periodically repeated cubic sample, consisting of $N = l^3$ particles, $l = 10,12,16,20,24$; calculations were run in cascade, in order of increasing temperature; each cycle (or sweep) consisted of N MC steps, and the finest temperature step used was $\Delta T^* = 0.001$, in the transition region. Equilibration runs took between 25 000 and 100 000 cycles, and production runs took between 500 000 and 3 500 000 (at least 2 500 000 cycles in the transition region, including the additional simulations mentioned below); macrostep averages for evaluating statistical errors were taken over 1000 cycles. Calculated thermodynamic quantities include mean potential energy per site U^* and configurational specific heat per particle C^*, where the asterisks mean scaling by ϵ and k_B, respectively.

As for structural characterization, we analyzed one configuration every cycle, by calculating both second- and fourth-rank ordering tensors $\mathcal{T}^{(L)}, L = 2,4$ [74–78] as well as corresponding rotation-invariant order parameters O_L. In other words, for $L = 2$,

$$\mathcal{T}_{\iota\kappa}^{(2)} = Q_{\iota\kappa} = \frac{1}{2}(3F_{\iota\kappa} - \delta_{\iota\kappa}), \quad (13)$$

$$F_{\iota\kappa} = \frac{1}{N}\sum_{j=1}^{N}(w_{j,\iota}w_{j,\kappa}); \quad (14)$$

the calculated $\mathbf{Q}$ tensor can be diagonalized; let $\{q_k, k = 1,2,3\}$ denote its real eigenvalues, let q' denote the eigenvalue with maximum magnitude, and let $q_{\max}$ denote the maximum. eigenvalue; moreover

$$\mathbf{Q} : \mathbf{Q} = \mathrm{tr}(\mathbf{Q} \cdot \mathbf{Q}) = \sum_{k=1}^{3} q_k^2, \quad (15)$$

where : denotes the contracted product. The fourth-rank counterpart is defined by

$$\begin{aligned}
\mathcal{T}_{\iota\kappa\lambda\mu}^{(4)} &= B_{\iota\kappa\lambda\mu} \\
&= \tfrac{1}{8}[35G_{\iota\kappa\lambda\mu} - 5(\delta_{\iota\kappa}F_{\lambda\mu} + \delta_{\iota\lambda}F_{\kappa\mu} + \delta_{\iota\mu}F_{\kappa\lambda} \\
&\quad + \delta_{\kappa\lambda}F_{\iota\mu} + \delta_{\kappa\lambda}F_{\iota\mu} + \delta_{\lambda\mu}F_{\iota\kappa}) + (\delta_{\iota\kappa}\delta_{\lambda\mu} + \delta_{\iota\lambda}\delta_{\kappa\mu} \\
&\quad + \delta_{\iota\mu}\delta_{\kappa\lambda})],
\end{aligned} \quad (16)$$

where

$$G_{\iota\kappa\lambda\mu} = \frac{1}{N}\sum_{j=1}^{N}(w_{j,\iota}w_{j,\kappa}w_{j,\lambda}w_{j,\mu}). \quad (17)$$

The corresponding frame-independent (rotationally invariant) order parameters are defined by

$$O_L = \sum_{j=1}^{N}\sum_{k=1}^{N} P_L(\mathbf{w}_j \cdot \mathbf{w}_k) \geqslant 0, \quad (18)$$

where the inequality follows from the addition theorem for spherical harmonics [79]; the order parameters of a configuration are thus defined by

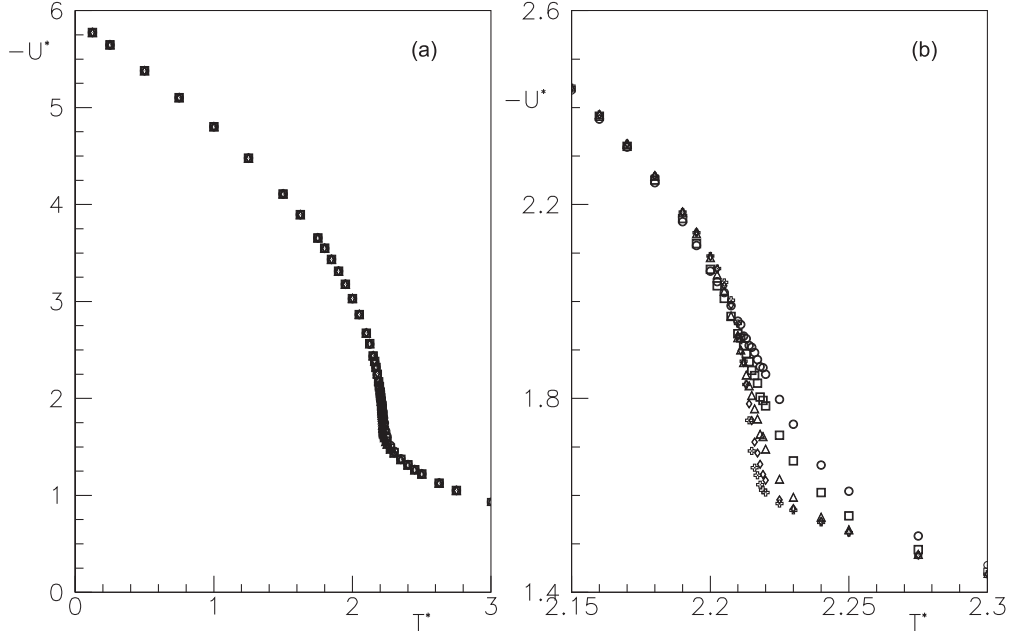$$\tau_L = \frac{1}{N}\sqrt{O_L}, \quad (19)$$

FIG. 1. Simulation results for the potential energy, obtained with different sample sizes. Meaning of symbols: circles: $l = 10$; squares: $l = 12$; triangles: $l = 16$; diamonds: $l = 20$, crosses: $l = 24$. Here and in the following figures, with the exception of simulation results for C^*, the statistical errors mostly fall within symbol sizes. Here as well as for Figs. 2, 5, and 6, panel a covers the whole investigated temperature range, and panel b presents the transition region in greater detail.

overall averages over the simulation chain are

$$\overline{\tau}_L = \frac{1}{N}\langle\sqrt{O_L}\rangle, \tag{20}$$

and the associated susceptibilities read

$$\chi_L = \frac{1}{N}\beta(\langle O_L \rangle - \langle\sqrt{O_L}\rangle^2), \tag{21}$$

where $\beta = 1/T^*$.

Notice that, by the addition theorem for spherical harmonics [79], Eq. (18) can actually be calculated [24,33,39] via the computationally more convenient single-particle sums

$$\xi_{L,m} = \sum_{j=1}^{N}\Re[Y_{L,m}(\mathbf{w}_j)], \quad \eta_{L,m} = \sum_{j=1}^{N}\Im[Y_{L,m}(\mathbf{w}_j)]; \tag{22}$$

here $m = 0,1,2,\ldots L$, $Y_{L,m}(\ldots)$ are spherical harmonics, and $\Re$ and $\Im$ denote real and imaginary parts, respectively; in turn,
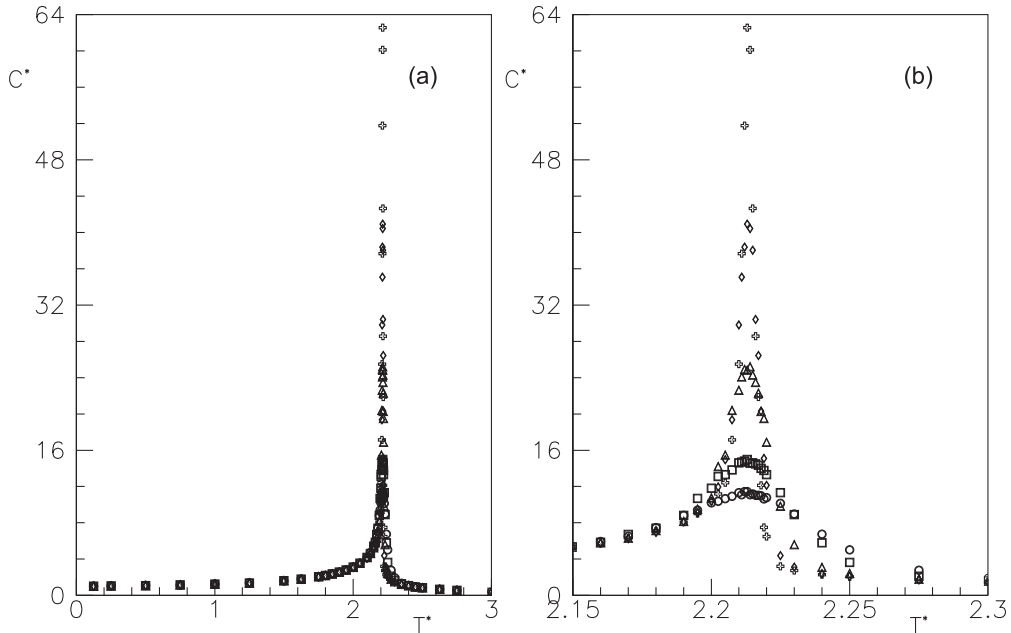

FIG. 2. Simulation results for the configurational specific heat C^*, obtained with different sample sizes; same meaning of symbols as in Fig. 1. The associated statistical errors, not shown, range between 1% and 5%.
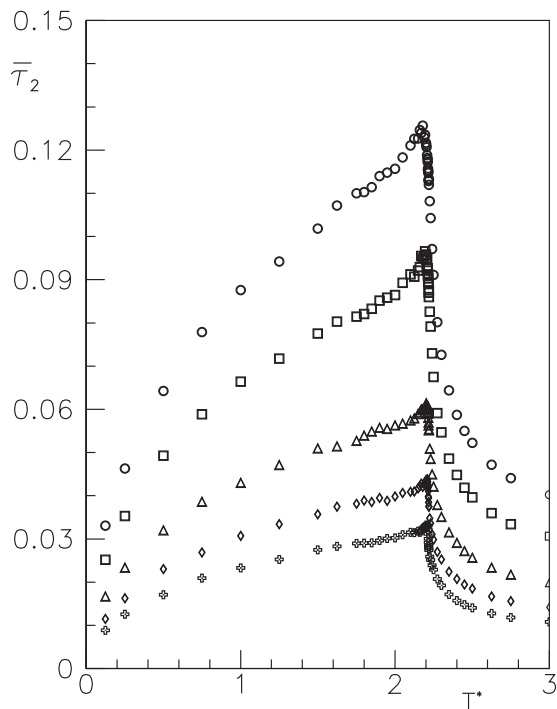
FIG. 3. Simulation results for the orientational order parameter $\overline{\tau}_2$, obtained with different sample sizes; same meaning of symbols as in Fig. 1.
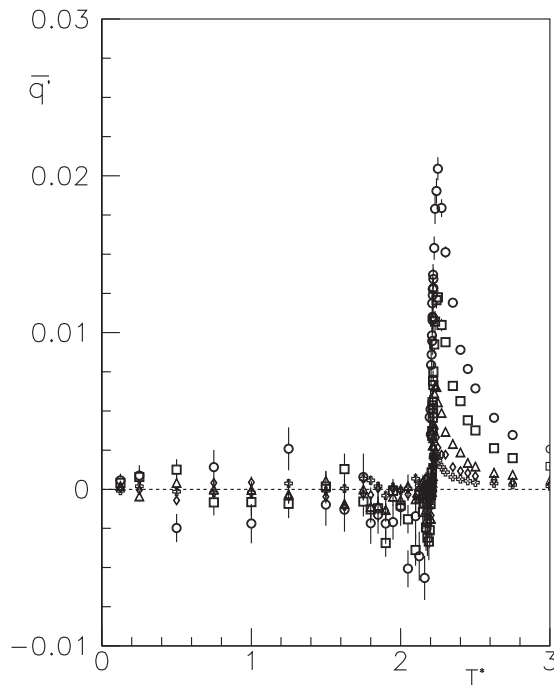

FIG. 4. Simulation results for the orientational order parameter $\overline{q'}$, obtained with different sample sizes; same meaning of symbols as in Fig. 1.

each spherical harmonic is a suitable polynomial constructed in terms of Cartesian components of the corresponding unit vector (see, e.g., Ref. [80]).

Moreover,

$$O_2 = \frac{2}{3}(\mathsf{Q} : \mathsf{Q}) = \frac{2}{3}\sum_{k=1}^{3} q_k^2, \tag{23}$$

$$O_4 = \frac{8}{35}(\mathsf{B} : \mathsf{B}). \tag{24}$$

There exist a few different but related possible measures of second-rank order; i.e., in addition to τ_2, one can consider the eigenvalues q_{max} or q', with $O_2 = |q'|^2$ in the uniaxial case; τ_2 and q_{max} have a definite sign, whereas the sign
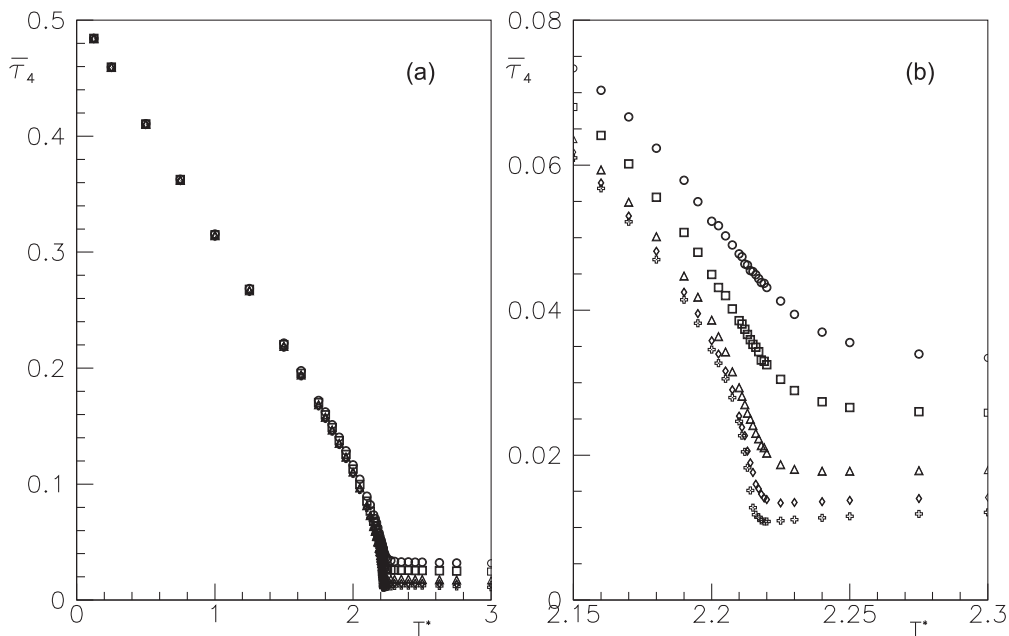

FIG. 5. Simulation results for the orientational order parameter $\overline{\tau}_4$ obtained with different sample sizes; same meaning of symbols as in Fig. 1.
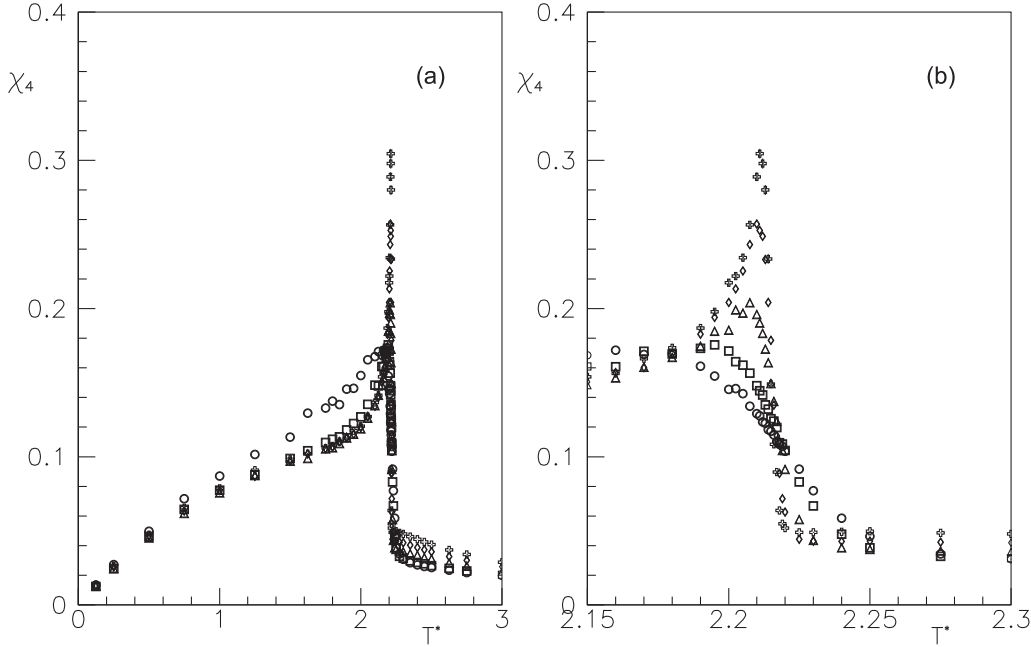
FIG. 6. Simulation results for the susceptibility χ_4, obtained with different sample sizes; same meaning of symbols as in Fig. 1.

of q' may fluctuate in the course of simulation, and better take into account configurations with antinematic order; for example, D_2-type configurations (Appendix A) yield $q' = -1/2$, $q_{max} = +1/4$, $\tau_2 = +1/2$.

For $L = 4$, the above $\mathcal{T}^{(4)}$ tensor can be copied ("folded") into a real, symmetric, and traceless matrix of order 9, say,
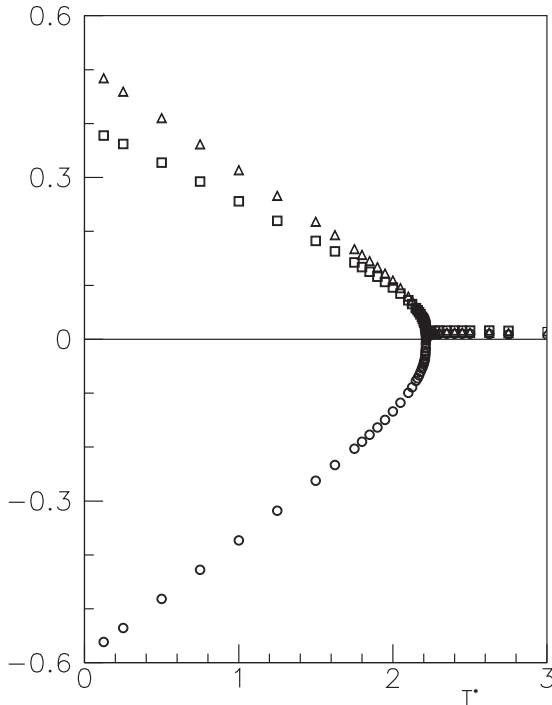

FIG. 7. Comparison between different definitions of the fourth-rank order parameter, based on simulation results obtained for the largest investigated sample size $l = 24$. Meaning of symbols: circles $\overline{\zeta}'$; squares: $\overline{\zeta}_{max}$; triangles: $\overline{\tau}_4$.

H [40,81,82], where, for example,

$$H_{\nu\rho} = B_{\iota\kappa\lambda\mu}, \quad \nu = 3(\iota - 1) + \lambda, \quad \rho = 3(\kappa - 1) + \mu \tag{25}$$

and

$$\mathcal{T}^{(4)} : \mathcal{T}^{(4)} = \mathsf{H} : \mathsf{H}. \tag{26}$$

The matrix H can be diagonalized to give the real eigenvalues $\{\zeta_k, k = 1, 2, \ldots, 9\}$; thus

$$O_4 = \frac{8}{35} \sum_{k=1}^{9} \zeta_k^2. \tag{27}$$

Here also there exist a few different and related possible measures of fourth-rank order, i.e., in addition to τ_4, one can consider the eigenvalue ζ' with maximum absolute value, or the maximum eigenvalue ζ_{max}. Besides the above procedure [Eq. (25)], other computational definitions of fourth-rank orientational order are also possible [30].

In principle, the same spin configuration might exhibit (or the same underlying interaction model might produce) different types of ordering, and the above definitions make it possible to calculate them independently of one another, in contrast to usual procedures for order parameters in nematic liquid crystals, where the definition of $\overline{P}_4$ and higher-order terms is physically bound to the director frame [75–77]. A few spin configurations possessing fourth-rank but no second-rank orientational order are presented in Appendix B, and their ordering quantities are summarized in Table I; for D_3-type configurations, $\tau_4 = \sqrt{21}/9 \approx 0.5092$.

IV. RESULTS

Simulation results for the potential energy U^* (Fig. 1) appeared to exhibit a gradual monotonic change with temperature; they were found to be independent of sample size up to

TABLE I. Eigenvalues of H [Eq. (25)] for the four discussed spin configurations.

Case	Number of spins	ζ_-	ζ_+	τ_4
1	6	$-7/12 \approx -0.5833$	$+7/8 = +0.875$	$\sqrt{21}/6 \approx 0.7638$
2	8	$-7/12 \approx -0.5833$	$+7/18 \approx +0.3889$	$\sqrt{21}/9 \approx 0.5092$
3	12	$-7/32 = -0.21875$	$+7/48 \approx +0.14583$	$\sqrt{21}/24 \approx 0.1909$
4	26	$-49/624 \approx -0.0785$	$+49/936 \approx +0.0523$	$7\sqrt{21}/468 \approx 0.0685$

$T_1^* \approx 2.2$ and then above $T_2^* \approx 2.3$; their overall temperature behavior suggested a change of slope at some intermediate temperature ≈ 2.21.

The configurational specific heat C^* (Fig. 2) was also found to be unaffected by sample size outside the named temperature range $[T_1^*, T_2^*]$; in that range sample-size effects became quite
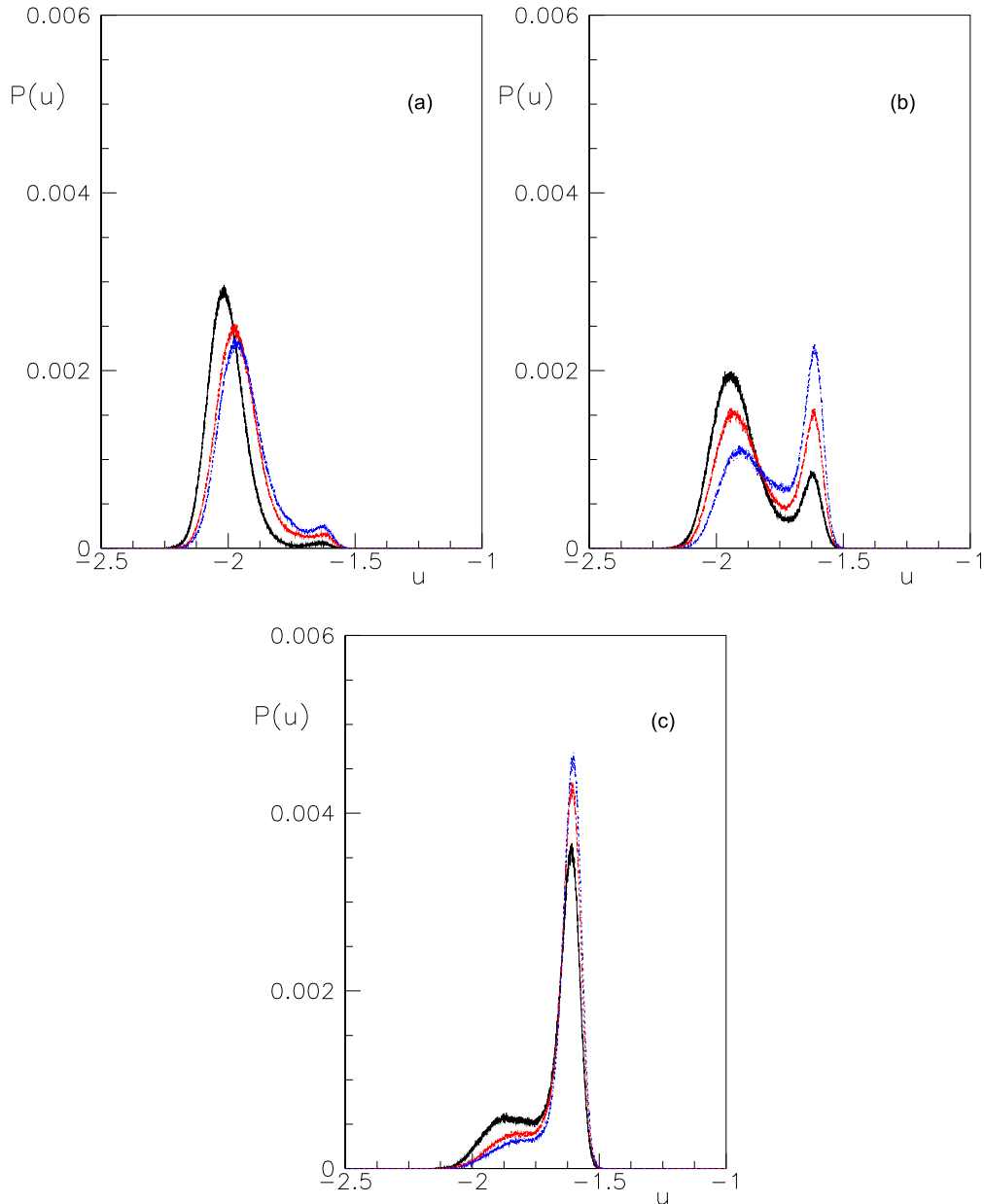

FIG. 8. Histograms of the single-particle potential energy u, obtained for $l = 24$ and different temperatures in the transition region. Meaning of symbols for panel (a): black continuous line: $T^* = 2.2075$; red dashed line: $T^* = 2.210$; blue dashed-dotted line: $T^* = 2.211$. Meaning of symbols for panel (b): black continuous line: $T^* = 2.212$; red dashed line: $T^* = 2.213$; blue dashed-dotted line: $T^* = 2.214$. Meaning of symbols for panel (c): black continuous line: $T^* = 2.215$; red dashed line: $T^* = 2.216$; blue dashed-dotted line: $T^* = 2.217$.

FIG. 9. Histograms of the fourth-rank order parameter τ_4, obtained for $l = 24$ and different temperatures in the transition region. Meaning of symbols for panel (a): black continuous line: $T^* = 2.2075$; red dashed line: $T^* = 2.210$; blue dashed-dotted line: $T^* = 2.211$. Meaning of symbols for panel (b): black continuous line: $T^* = 2.212$; red dashed line: $T^* = 2.213$; blue dashed-dotted line: $T^* = 2.214$. Meaning of symbols for panel (c): black continuous line: $T^* = 2.215$; red dashed line: $T^* = 2.216$; blue dashed-dotted line: $T^* = 2.217$.
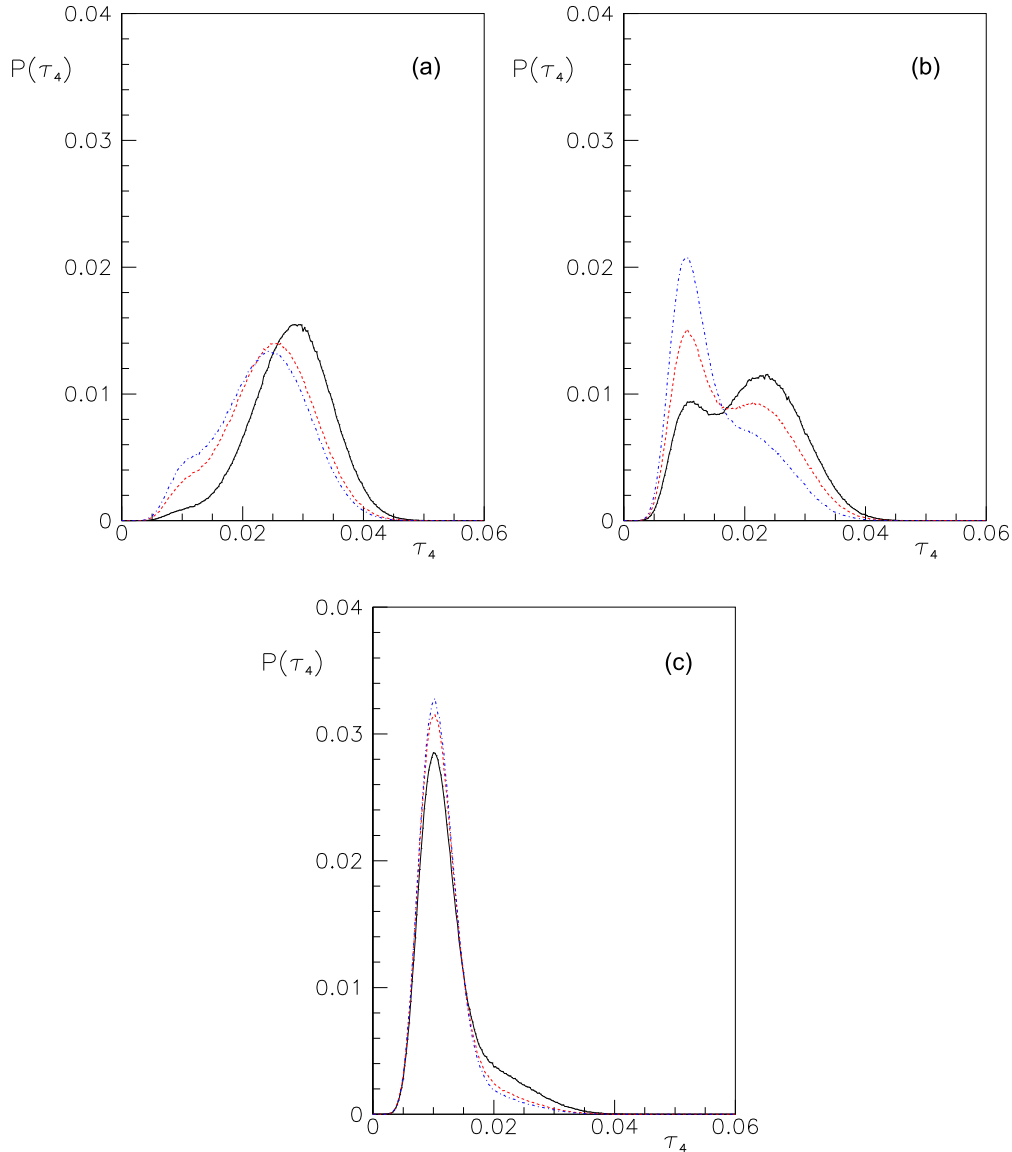
apparent, and a peak was found to develop at ≈ 2.21, growing narrower and higher with increasing sample size. The second-rank order parameter $\overline{\tau}_2$ was calculated as well; at all examined temperatures, the results were found to keep decreasing with increasing sample size on the other hand, for all examined sample sizes, they were found to increase with temperature, reach a maximum in the transition region, and then decrease with increasing temperature (Fig. 3).

Notice that configurations possessing some amount of second-rank orientational order may have potential energies not too high above the ground state of the model under investigation here (Sec. II and Appendix A); in the low-temperature ordered and in the transition regions they can be favored by thermal fluctuations; in turn, at a given temperature, thermal fluctuations tend to be reduced with increasing sample size. On the other hand, as pointed out in the previous

section, there are different possible computational measures of second-rank order for a configuration; usage of q' yielded absolute values smaller by roughly an order of magnitude, and sometimes negative signs in the ordered region, as shown in Fig. 4. The corresponding susceptibility χ_2 (not shown) was found to be less affected by sample size.

Simulation results for the fourth-rank order parameter $\overline{\tau}_4$ were found to be independent of sample size up to $T^* \approx 2.1$, and then developed a recognizable decrease with increasing sample size; their overall temperature behavior seemed to suggest a continuous evolution with temperature (Fig. 5).

Simulation results for the corresponding susceptibility χ_4 were found to increase with temperature (and to be unaffected by sample sizes for $l > 10$) up to the above transition region, where a peak developed, growing higher and narrower with increasing sample size (Fig. 6).

As pointed out in Sec. III, different measures of fourth-rank orientational order can be defined, involving τ_4, ζ', or $\zeta_{\max}$, respectively; simulation results obtained for the three definitions and with the largest investigated sample size $l = 24$ are compared in Fig. 7, where the three definitions appear to be mutually compatible; ratios between pairs of them (at the same temperature) were also calculated, and found to evolve slowly with temperature in the ordered region, where they remained close to their ground-state values (see also Appendix B).

The above results point to a transition between cubatic and isotropic phase, taking place at $T^* \approx 2.213$; in order to obtain some more evidence of its thermodynamic character, histograms for the frequency distribution $P(u)$ (where u denotes the scaled potential energy per particle, and $U^* = \langle u \rangle$) as well as for $P(\tau_4)$ (see, e.g., Refs. [47,83,84]) were calculated in the transition region ($T^* = 2.2075, 2.210$ to 2.220 with step 0.001, $T^* = 2.225$), for all examined sample sizes, over additional run lengths ranging between $1\,000\,000$ and $1\,500\,000$ cycles, and by analyzing one configuration every cycle. Results for $P(u)$ and $l = 24$ at selected temperatures are plotted in Fig. 8, and their counterparts for $P(\tau_4)$ are reported in Fig. 9. The width of the distribution $P(u)$ as measured by the variance (not shown) was found to shrink with increasing sample size; the double-peaked structure in Fig. 8(b) only developed for $l \geqslant 16$, and the peaks appeared to grow higher and narrower with increasing sample size. As for $P(\tau_4)$, the width of the distribution was found to shrink with increasing sample size as well, and the double-peaked structure in Fig. 9(b) developed only for $l \geqslant 20$. In both cases, histograms obtained at higher temperatures, not shown, exhibited rather narrow single peaks; thus histograms obtained for large samples exhibit a two-peak structure over a rather narrow temperature range, pointing to a weak first-order transition taking place at $T \approx 2.213$.

V. CONCLUSIONS

We have carried out a MC simulation study of a lattice model consisting of uniaxial ($D_{\infty h}$-symmetric) particles coupled by long-range dispersion interactions of the LHB type; in the named setting the model becomes equivalent to its NS counterpart; the model was found to support no second-rank order but to possess fourth-rank order in its low-temperature phase; simulation results point to a weak first-order transition whose transition temperature is estimated to be $T_c^* = 2.213 \pm 0.002$, where the uncertainty is conservatively taken to be twice the temperature step used in the transition region. Let us recall that the n-n counterpart supports [63,71] a first-order transition to a nematically ordered phase, taking place at 2.238 ± 0.001; the n-n model is reasonably well described by a MF treatment of the MS type, predicting a transition temperature 2.6424; as already pointed out in Ref. [65], a MF treatment of the MS type could be applied in this case as well: it would produce the same pseudopotential as in the n-n case (within a scaling factor), but here it would be physically wrong.

The investigated potential model involves second-rank interaction terms and produces no second-rank but only fourth-rank orientational order; it may be appropriate to mention that a few other potential models are known in the literature, where interactions of a certain rank produce only higher-rank correlations or even long-range orientational order: more

explicitly, they are classical lattice-spin models involving two- or three-component unit vectors coupled by competing and frustrating first-rank (magnetic) interactions, which may result in second-rank correlations or even long-range order at finite temperature [85–87]; this appears to happen via a mechanism of entropic selection (order by disorder) of ground-state configurations, in contrast to the energetic effects acting here (Sec. II).

There are also a few related interaction models involving uniaxial particles and which seem to be worth examining or revisiting in terms of cubatic orientational order. On the one hand, one can study the effect of lattice geometry, by addressing BCC and FCC counterparts of the present simple-cubic lattice model; one could even give up the lattice, allow particle centers to move in $\mathbb{R}^3$, and supplement the present interaction model with a purely radial term enforcing some minimum distance between particle centers (the "liquid" setting. for short); there is a continuum counterpart of Eq. (9):

$$\int P_2(\mathbf{w} \cdot \mathbf{v}) d^2\mathbf{v} = 0, \tag{28}$$

where the unit vector $\mathbf{w}$ is assigned and integration over the unit vector $\mathbf{v}$ is carried out on the whole unit sphere with the usual uniform measure: this formula suggests that, in the "liquid" setting, the S_{jk} terms (see Sec. II) should largely cancel out upon summing over all interacting pairs, provided that the distribution of intermolecular vectors is essentially isotropic.

Interaction models involving just linear point quadrupoles associated with a 3D lattice were studied some 40 years ago, analytically [88–91] and by classical simulations [92,93], as simplified models of solid nitrogen [94], and might now be revisited, also in terms of overall fourth-rank orientational order. For example, the low-temperature, room-pressure α phase of solid nitrogen is usually assumed to belong to space group $Pa3$ (but space group $P2_13$ is also possible [94,95]). The $Pa3$ structure involves particle centers associated with a FCC lattice, where the four particles in the cubic unit cell are oriented along the body diagonals, thus producing no overall second-rank orientational order, and a finite amount of its fourth-rank counterpart, actually the same ground-state value $\tau_4 = \sqrt{21}/9$ as in our case (see also Appendix B); in some original simulation papers a local (sublattice-wise) second-rank order parameter was defined with respect to the corresponding ground-state orientations [92,93].

We hope to address some of these points in the near future.

APPENDIX A: GROUND STATE CONFIGURATION

Let (X, Y, Z) denote the Cartesian components of a unit vector, parameterized by two polar angles (Θ, Φ); for the generic lattice site $\mathbf{x}_j$ let h, k, l denote the integer coordinate

(we write h instead of h_j for simplicity of notation), then, for each site j [65]:

$$\mathbf{w}_j = (-1)^{k+l} X \mathbf{e}_1 + (-1)^{h+l} Y \mathbf{e}_2 + (-1)^{h+k} Z \mathbf{e}_3. \quad (A1)$$

A few configurations defined by special cases of Eq. (A1) are the following:

(1) D_1 ($X = Y = 0, Z = 1$), with full orientational order along a lattice axis

(2) D_2 ($X = Y = \sqrt{2}/2, Z = 0$), with a negative second-rank order parameter $(-1/2)$ (antinematic order)

(3) D_3 ($X = Y = Z = \sqrt{3}/3$), possessing no second-rank but a finite amount of fourth-rank order.

Let W_1^*, W_2^*, W_3^* denote the corresponding potential energies per particle, where the asterisk means scaling by ϵ; known results when the interaction was truncated at n-n separation [63,65,71] are

$$W_1^* = -6 < W_2^* = -21/4 < W_3^* = -5; \quad (A2)$$

on the other hand, when the interaction was extended to next-nearest or more distant neighbors, the sequence became [65]

$$W_3^* < W_2^* < W_1^*, \quad (A3)$$

and the three values were found to be much closer to one another; notice also that D_2-type configurations become favoured over D_1-type. Different truncation radii were tried, and found to slightly change the three individual values, but not the inequalities among them; for example, truncation by the condition $\mathbf{r} \cdot \mathbf{r} \leqslant 25$ yielded

$$W_1^* = -5.813, \quad W_2^* = -5.879, \quad W_3^* = -5.900; \quad (A4)$$

the configuration potential energy was also calculated over a finer angular grid in (Θ, Φ), and results appeared to confirm D_3 as ground-state candidate; moreover, and more importantly, simulations carried out at low temperatures, starting from any of the three above configurations, or even for a randomly generated one, quickly gave results corresponding to a mild thermal evolution of D_3, as originally found by simulation in Ref. [64].

APPENDIX B: SIMPLE SPIN CONFIGURATIONS POSSESSING FOURTH-RANK BUT NO SECOND-RANK ORDER

On can construct a few simple spin configurations, possessing, fourth-rank (cubic) order but no second-rank (nematic) one, and for which all odd-rank ordering tensors vanish;

(1) A first example involves 6 unit vectors oriented along $\pm \mathbf{e}_\iota, \iota = 1, 2, 3$;

(2) A second example consists of eight unit vectors with Cartesian components $\pm \sqrt{3}/3$ (all combinations of signs) and corresponds to the ground state for the interaction model under investigation here; actually, this configuration consists of two disjoint subsets, composed of four spins whose components have an even number of negative signs, and four spins with an odd number of negative signs, respectively; for both subsets and for the whole configuration, $\tau_1 = \tau_2 = 0, \tau_4 = \sqrt{21}/9$; moreover, for each subset, $\tau_3 = \sqrt{5}/3 \approx 0.7454$;

(3) A third example involves 12 unit vectors with Cartesian components obtained from $(0, \pm \sqrt{2}/2, \pm \sqrt{2}/2)$ by applying all possible combinations of signs and all possible permutations;

(4) One can build a 26 spin configuration as union of the three above cases.

In all four cases the above matrix H [Eq. (25)] was found to possess the eigenvalue 0 with degeneracy 4, as well as two other nonzero ones, with opposite signs (ζ_- and ζ_+ in the following), degeneracies 2 or 3, respectively, and absolute values in the corresponding ratio (the eigenvalue with smaller magnitude possessing higher degeneracy); moreover we found $\zeta' > 0$ for the first case, and $\zeta' < 0$ in all others (see also Table I); thus, in all the four cases,

$$\tau_4 = \sqrt{(8/35) \sum_{k=1}^{9} \zeta_k^2}, \quad \sum_{k=1}^{9} \zeta_k^2 = (10/3)|\zeta'|^2,$$

$$\tau_4/|\zeta'| = (4/21)\sqrt{21} \approx 0.8728$$

.

---

[1] G. R. Luckhurst, Nature (London) **430**, 413 (2004).

[2] G. R. Luckhurst and T. J. Sluckin (eds.), *Biaxial Nematic Liquid Crystals Theory, Simulation, and Experiment* (Wiley, New York, 2015).

[3] T. R. Taylor, J. L. Fergason. and S. L. Arora, Phys. Rev. Lett. **24**, 359 (1970).

[4] M. J. Freiser, Phys. Rev. Lett. **24**, 1041 (1970).

[5] G. R. Luckhurst and T. J. Sluckin, in *Biaxial Nematic Liquid Crystals Theory, Simulation, and Experiment*, edited by G. R. Luckhurst and T. J. Sluckin (Wiley, New York, 2015), Chap. 15.

[6] M. Lehmann, in *Biaxial Nematic Liquid Crystals Theory, Simulation, and Experiment*, edited by G. R. Luckhurst and T. J. Sluckin (Wiley, New York, 2015), Chap. 14.

[7] M. V. Jarić, Nucl. Phys. B **265**, 647 (1986).

[8] L. G. Fel, Phys. Rev. E **52**, 702 (1995).

[9] L. G. Fel, Phys. Rev. E **52**, 2692 (1995).

[10] B. Mettout, Phys. Rev. E **74**, 041701 (2006).

[11] J. Nissinen, K. Liu, R.-J. Slager, K. Wu, and J. Zaanen, Phys. Rev. E **94**, 022701 (2016).

[12] S. Torquato and F. H. Stillinger, Rev. Mod. Phys. **82**, 2633 (2010).

[13] U. Agarwal and F. A. Escobedo, Nat. Mater. **10**, 230 (2011).

[14] J. de Graaf, R. van Roij, and M. Dijkstra, Phys. Rev. Lett. **107**, 155501 (2011).

[15] S. Torquato and Y. Jiao, Phys. Rev. E **86**, 011102 (2012).

[16] P. F. Damasceno, M. Engel, and S. C. Glotzer, Science **337**, 453 (2012).

[17] D. Chen, Y. Jiao, and S. Torquato, J. Phys. Chem. B **118**, 7981 (2014).

[18] A. P. Gantapara, J. de Graaf, R. van Roij, and M. Dijkstra, J. Chem. Phys. **142**, 054904 (2015).

[19] L. Radzihovsky and T. C. Lubensky, Europhys. Lett. **54**, 206 (2001).

[20] T. C. Lubensky and L. Radzihovsky, Phys. Rev. E **66**, 031704 (2002).

[21] P. E. Cladis, H. R. Brand, and H. Pleiner, Liquid Crystals Today **9**, 1 (1999).

[22] H. R. Brand, P. E. Cladis, and H. Pleiner, Europhys. Lett. **57**, 368 (2002).

[23] H. R. Brand, P. E. Cladis, and H. Pleiner, Ferroelectrics **315**, 165 (2005).

[24] S. Romano, Phys. Rev. E **77**, 021704 (2008).

[25] L. Longa, G. Pająk, and T. Wydro, Phys. Rev. E **79**, 040701(R) (2009).

[26] K. Trojanowski, G. Pająk, L. Longa, and T. Wydro, Phys. Rev. E **86**, 011704 (2012).

[27] G. Pelzl, S. Diele, and W. Weissflog, Adv. Mater. **11**, 707 (1999).

[28] J. Matraszek, J. Mieczkowski, J. Szydłowska, and E. Gorecka, Liq. Cryst. **27**, 429 (2000).

[29] D. Wiant, K. Neupane, S. Sharma, J. T. Gleeson, S. Sprunt, A. Jákli, N. Pradhan, and G. Iannacchione, Phys. Rev. E **77**, 061701 (2008)

[30] J. A. C. Veerman and D. Frenkel, Phys. Rev. A **45**, 5632 (1992).

[31] A. Chamoux and A. Perera, J. Chem. Phys. **108**, 8172 (1998).

[32] A. Chamoux and A. Perera, Phys. Rev. E **58**, 1933 (1998).

[33] R. Blaak, D. Frenkel, and B. M. Mulder, J. Chem. Phys. **110**, 11652 (1999).

[34] R. Blaak and B. M. Mulder, Phys. Rev. E **58**, 5873 (1998).

[35] R. Blaak, B. M. Mulder, and D. Frenkel, J. Chem. Phys. **120**, 5486 (2004).

[36] B. S. John, A. Stroock, and F. A. Escobedo, J. Chem. Phys. **120**, 9383 (2004).

[37] B. S. John, A. Stroock, and F. A. Escobedo, J. Phys. Chem. B **109**, 23008 (2005).

[38] B. S. John, C. Juhlin, and F. A. Escobedo, J. Chem. Phys. **128**, 044909 (2008).

[39] S. Romano, Phys. Rev. E **74**, 011704 (2006).

[40] P. D. Duncan, M. Dennison, A. J. Masters, and M. R. Wilson, Phys. Rev. E **79**, 031702 (2009).

[41] P. D. Duncan, A. J. Masters, and M. R. Wilson, Phys. Rev. E **84**, 011702 (2011).

[42] M. Marechal, A. Patti, M. Dennison, and M. Dijkstra, Phys. Rev. Lett. **108**, 206101 (2012).

[43] M. R. Wilson, P. D. Duncan, M. Dennison, and A. J. Masters, Soft Matter **8**, 3348 (2012).

[44] H. N. W. Lekkerkerker and G. J. Vroege, Philos. Trans. R. Soc. London A **371**, 20120263 (2013).

[45] S. J. S. Qazi, G. Karlsson, and A. R. Rennie, J. Colloid Interface Sci. **348**, 80 (2010).

[46] G. Lasher, Phys. Rev. A **5**, 1350 (1972).

[47] P. A. Lebwohl and G. Lasher, Phys. Rev. A **6**, 426 (1972); **7**, 2222 (1973).

[48] P. Pasini, C. Chiccoli, and C. Zannoni, *Advances in the Computer Simulations of Liquid Crystals*, edited by P. Pasini and C. Zannoni, NATO Science Series (Kluwer, Dordrecht, 2000), Vol. C 545, Chap. 5.

[49] M. A. Bates and G. R. Luckhurst, Phys. Rev. E **72**, 051702 (2005).

[50] W. Maier and A. Saupe, Z. Naturforschg. **13a**, 564 (1958); **14a**, 882 (1959); **15a**, 287 (1960).

[51] G. R. Luckhurst, *The Molecular Physics of Liquid Crystals*, edited by G. R. Luckhurst and G. W. Gray (Academic Press, London, 1979), Chap. 4.

[52] G. R. Luckhurst, in *Physical Properties of Liquid Crystals: Nematics*, edited by D. A. Dunmur, A. Fukuda, and G. R. Luckhurst (INSPEC, London, 2001), Chap. 2.1.

[53] C. G. Gray and K. E. Gubbins, *Theory of Molecular Fluids, vol. 1: Fundamentals* (Oxford University Press, Oxford, 1984).

[54] A. J. Stone, *The Theory of Intermolecular Forces* (Oxford University Press, Oxford, 1997).

[55] F. London, Trans. Faraday Soc. **33**, 8 (1937).

[56] J. H. de Boer and G. Heller, Physica **4**, 1045 (1937).

[57] J. de Boer, Physica **9**, 363 (1942).

[58] A. J. van der Merwe, Z. Phys. **196**, 212 (1966); **196**, 332 (1966).

[59] B. C. Kohin, J. Chem. Phys. **33**, 882 (1960).

[60] S. L. Price and A. J. Stone, Mol. Phys. **40**, 805 (1980).

[61] E. Burgos, C. S. Murthy, and R. Righini, Mol. Phys. **47**, 1391 (1982).

[62] R. A. Kromhout and B. Linder, J. Phys. Chem. **99**, 16909 (1995).

[63] R. L. Humphries, G. R. Luckhurst, and S. Romano, Mol. Phys. **42**, 1205 (1981).

[64] P. Simpson, Ph.D. thesis, University of Southampton, Southampton, UK, 1982.

[65] S. Romano, Liq. Cryst. **3**, 323 (1988).

[66] M. A. Bates, Phys. Rev. E **65**, 041706 (2002).

[67] S. Romano, Physica A **322**, 432 (2003).

[68] J. Nehring and A. Saupe, J. Chem. Phys. **54**, 337 (1971); **56**, 5527 (1972).

[69] G. Vertogen and W. H. de Jeu, *Thermotropic Liquid Crystals, Fundamentals* (Springer Verlag, Berlin, 1988).

[70] G. Barbero and R. Barberi, in *Physics of Liquid Crystalline Materials*, edited by I.-C. Khoo and F. Simoni (Gordon and Breach, Philadelphia, 1991), Chap. 8.

[71] R. Hashim and S. Romano, Int. J. Mod. Phys. B **13**, 3879 (1999).

[72] S. Romano, Mod. Phys. Lett. B **15**, 137 (2001).

[73] S. Romano, Phys. Lett. A **305**, 196 (2002).

[74] A. D. Buckingham, Discuss. Faraday Soc. **43**, 205 (1967).

[75] C. Zannoni, in *The Molecular Physics of Liquid Crystals*, edited by G. R. Luckhurst and G. W. Gray (Academic Press, London, 1979), Chap. 3.

[76] C. Zannoni, in *The Molecular Physics of Liquid Crystals*, edited by G. R. Luckhurst and G. W. Gray (Academic Press, London, 1979), Chap. 9.

[77] C. Zannoni, in *Advances in the Computer Simulations of Liquid Crystals*, edited by P. Pasini and C. Zannoni, NATO Science Series (Kluwer, Dordrecht, 2000), Vol. C 545, Chap. 2.

[78] S. S. Turzi, J. Math. Phys. **52**, 053517 (2011).

[79] G. B. Arfken and H. J. Weber, *Mathematical Methods for Physicists*, 4th ed. (Academic Press, San Diego, 1995).

[80] J. W. Leech and D. J. Newman, *How to Use Groups* (Methuen, London, 1969).

[81] K. Zheng and P. Palffy-Muhoray, Electronic-liquid crystal communications (2007), http://www.e-lc.org/docs/2007_02_03_02_33_15.

[82] J. Geng and J. V. Selinger, Phys. Rev. E **80**, 011707 (2009).

[83] U. Fabbri and C. Zannoni, Mol. Phys. **58**, 763 (1986).

[84] C. Chiccoli, P. Pasini, and C. Zannoni, Physica A **148**, 298 (1988).

[85] J. T. Chalker, P. C. W. Holdsworth, and E. F. Shender, Phys. Rev. Lett. **68**, 855 (1992).

[86] R. Moessner and J. T. Chalker, Phys. Rev. B **58**, 12049 (1998).

[87] J. M. Hopkinson, S. V. Isakov, H.-Y. Kee, and Y. B. Kim, Phys. Rev. Lett. **99**, 037201 (2007).

[88] J. Felsteiner, D. B. Litvin, and J. Zak, Phys. Rev. B **3**, 2706 (1971).

[89] J. C. Raich, J. Chem. Phys. **56**, 2395 (1972).

[90] J. C. Raich and R. D. Etters, J. Low Temp. Phys. **7**, 449 (1972).

[91] J. Felsteiner and Z. Friedman, Phys. Rev. B **8**, 3996 (1973).

[92] M. J. Mandell, J. Chem. Phys. **60**, 1432 (1974); **60**, 4880 (1974).

[93] S. Romano, Z. Naturforschg. **29a**, 1631 (1974).

[94] T. A. Scott, Phys. Rep. **27**, 85 (1976).

[95] See, for example, http://rruff.geo.arizona.edu/AMS/minerals/Nitrogen.